The Effect of Infill Pattern and Density on the Response of 3-D-Printed Sensors Based on FBG Technology

D. Lo Presti, *Associate Member, IEEE*, C. Leitão, A. Noccaro, *Member, IEEE*, C. Tavares, C. Massaroni, *Senior Member, IEEE*, M. A. Caponero, P. Antunes, D. Formica, *Senior Member, IEEE*, and E. Schena, *Senior Member, IEEE*

***Abstract*—Fiber Bragg gratings (FBGs) are known for their uses in applications ranging from civil engineering to medicine. A bare FBG is small and light; hence, it can be easily embedded into hosting materials. However, conventional fabrication methods are generally time-consuming with reproducibility issues. A more recent strategy has been proposed to develop novel FBG-based systems by encapsulating the grating within 3-D-printed structures. This process, known as 3-D printing, is characterized by several advantages like rapid prototyping, printing precision, and high customization. The possibility of quickly personalizing the 3-D-printed sensors by customizing the infill settings makes this technique very appealing for medical purposes, especially for developing smart systems. However, the influence of printing settings on the sensor response has not been yet systematically addressed. This work aimed at combining FBG with the most popular 3-D printing technique (the fused deposition modeling [FDM]) to develop four 3-D-printed sensors with different printing profiles. We chose two patterns (triangle and gyroid) and two infill densities (30% and 60%) to investigate their influence on the sensors' response to strain, temperature, and relative humidity (RH), and on the hysteresis behavior. Then, we preliminary assess the sensor performance in a potential application scenario for FBG-based 3-D printing technology: the cardiorespiratory monitoring. The promising results confirm that our analysis can be considered the first effort to improve the knowledge about the influence of printing profiles on sensor performance and, consequently, pave the way to develop highly performant 3-D-printed sensors customized for specific applications.**

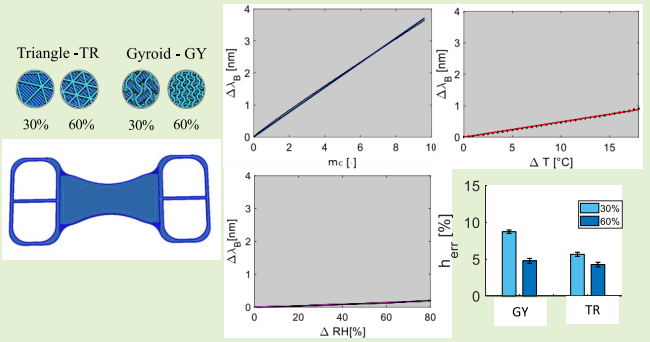

***Index Terms*—3-D printing technology, fiber Bragg grating (FBG) sensors, fused model deposition, infill properties, medical applications, metrological characterization, wearable systems.**

I. Introduction

FIBER Bragg gratings (FBGs) are the most popular passive fiber optic sensors [1]. FBGs and other optical sensors have been extensively used for a variety of sensing applications ranging from structural to human health monitoring, thanks to their numerous attractive features compared to electrical and piezoelectric sensors (e.g., miniaturized size, immunity to electromagnetic interferences, chemical inertia, high sensitivity, and multiplexing capability) [2], [3], [4], [5], [6].

In the case of FBGs, the need for an optical spectrum analyzer and the optical fiber brittleness has dampened their large-scale use, especially for wearable applications [3]. In recent years, advances in optical interrogators and the packaging of FBGs into hosting materials have been proposed to overcome the main issues with this technology, posing an exciting option for the design of more robust and usable FBG-based smart devices and structures. Many studies have focused on the encapsulation of FBGs into materials such as epoxy resins, ribbon tapes, and composites before the installation on bridges, ships, aircraft wings, and geotechnical objects [2], [7], [8], [9], [10]. Recently, the use of FBGs in medical applications

Manuscript received 22 July 2022; revised 18 August 2022; accepted 20 August 2022. Date of publication 5 September 2022; date of current version 14 October 2022. This work was supported in part by the FCT/MEC through the project i3N under Grant UIDB/50025/2020, Grant UIDP/50025/2020, and Grant LA/P/0037/2020; and in part by the H2020/ICT European Project "CONnected through roBOTS (CONBOTS): physically coupling humans to boost handwriting and music learning" under Grant ICT-09-2019-2020. The work of C. Leitão was supported by the FCT under Contract CEEIND/00154/2020. The associate editor coordinating the review of this article and approving it for publication was Dr. Rajan Jha. *(Corresponding author: E. Schena.)*

This work involved human subjects or animals in its research. Approval of all ethical and experimental procedures and protocols was granted by the Ethical Committee of Università Campus Bio-Medico di Roma under Protocol No. ST-UCBM 27.2(18).20.

Please see the Acknowledgment section of this article for the author affiliations.

Digital Object Identifier 10.1109/JSEN.2022.3202101

has led to the necessity of meeting more strict requirements in terms of overall system safety. Biocompatible and skin-like silicone elastomers (e.g., polydimethylsiloxane [PDMS] and Dragon Skin[1] silicones) have been proposed for packaging FBGs into flexible layers to develop wearables for vital signs monitoring and rehabilitation purposes [11], [12], [13], [14]. These sensors are characterized by high skin conformability and adaptability, but their fabrication process can be time-consuming since silicones take some time from their preparation to completely cure (from a few hours to more than two days at ambient temperature and humidity) and can require specific master molds to confer the chosen shape to the flexible matrix [4], [15], [16].

The rapid advancement of 3-D printing technology with its relatively low cost, rapid prototyping, and easy customization of the fabrication process can be brought to bear on these issues [17], [18]. The most attractive features of 3-D printing are the high repeatability, the good fabrication tolerance (both in dimensions and surface roughness), the rapid prototyping, and the customizable design. In fact, 3-D printing provides an opportunity to fine-tune the sensor structure by choosing several printing profiles to reach high performance [18]. Profiles in 3-D printing are a set of parameters, including printing orientation, materials selection, and overall design (shape, size, solid density, and pattern) [19]. When varying any of these settings, the obtained result may consequently be different in terms of structural properties [20]. The possibility of easily personalizing the printing profile makes the 3-D printing very appealing for medical purposes. Indeed, custom manufacturing can allow the development of FBG-based wearable systems to best suit the strict requirements of medical devices and meet the increasing demand for a personalized healthcare ecosystem [21], [22]. However, finding the perfect match among the plethora of available parameters to successfully apply 3-D printing in the fabrication of FBG-based systems is still challenging. Acquiring knowledge of the influence of the printing profile on the sensor response can provide more clarity on the optimum parameters to preset for the development of 3-D-printed cutting-edge sensors. Although the majority of works focused on 3-D-printed sensors use a specific printing profile, its role in the FBG metrological properties is largely overlooked. Only two studies investigated the influence of different infill densities on the FBG sensitivity to force, temperature (T) [23], and strain (ε) [24].

Another aspect to consider in the FBG encapsulation within 3-D structures is that the grating integration must be stable and secure. For this reason, most of the 3-D-printed sensors based on the FBG technology were fabricated by stopping the printer at one point (usually at half printing) to allow a secure placement of the optical fiber, and cyanoacrylate glue was often used to stick the FBG to the 3-D structure before resuming the printing. However, the use of a glue layer does not ensure high repeatability in the fabrication process, making the fiber encapsulation poorly controllable [24], [25].

The present study positions itself within the field of 3-D-printed sensors based on the FBG technology for medical applications. The potential scenarios may range from the monitoring of physiological parameters (e.g., breathing and heart beating) to the tracking of human activities (e.g., joint movements).

Here, we report the fabrication of four 3-D-printed sensors manufactured in thermoplastic polyurethane (TPU) with different infill patterns and densities to investigate the influence of these printing settings on the sensor response to ε, T, relative humidity (RH), and hysteresis. Finally, we assessed the feasibility of the use of the proposed sensors for instrumenting wearable systems. In particular, we investigated their use for monitoring cardiorespiratory activities.

The main advances introduced by this study rely on 1) the novelty in the technique proposed for the sensor fabrication since it does not require the use of glue. In this way, an improvement in the repeatability of the fabrication process should be reached and 2) the investigation of the influence of the main infill properties (i.e., density and pattern) on the sensor response. Given the multitude of settings and their effects on the performance of 3-D-printed sensors, our analysis can be considered as a first effort to improve the knowledge about the relationship between printing profile and sensor performance, an essential step to teasing out the appropriate way for tailoring the sensor design to specific applications.

II. FBG Technology (Background and Working Principles)

An FBG sensor is a permanent periodical perturbation in the refractive index of an optical fiber core. When an incident broadband light propagates through the grating, a narrow spectrum is reflected backward, while another part is transmitted with negligible attenuation [1]. The sharp reflected peak is centered at the Bragg wavelength, λ_B

$$\lambda_B = 2\, n_{\text{eff}}\, \Lambda \tag{1}$$

where n_{eff} is the effective refractive index of the fiber core at the grating and Λ is the periodicity of the grating. λ_B shifts when ε and T changes (ΔT) are applied to the grating. The shift of $\lambda_B(\Delta\lambda_B)$ is given by

$$\Delta\lambda_B = \lambda_B[(1 - P_e)\varepsilon + (\alpha_T + \zeta)\Delta T]. \tag{2}$$

The first term represents the $\Delta\lambda_B$ contribution due to ε with P_e the photoelastic constant of the fiber. The second term is related to the effect of T on the grating with α_T the thermal expansion coefficient and ζ the thermo-optic coefficient of the fiber.

The use of encapsulation materials (e.g., protective fiber coatings, silicones, or, more recently, 3-D printing matrices) may cause a change in the FBG response to ε and T since the mechanical and thermal properties of the material can affect the metrological characteristics of the sensor. Moreover, when the encapsulation material is hygroscopic, it may also experience volumetric changes caused by the moisture absorption and desorption and, in turn, induce an additional $\Delta\lambda_B$.

In this study, we packaged four commercial polyimide-coated FBG sensors into 3-D structures with different infill properties. TPU was used as a printing filament. Both polyimide and TPU are hygroscopic materials [26], [27]. For this

[1]Trademarked.

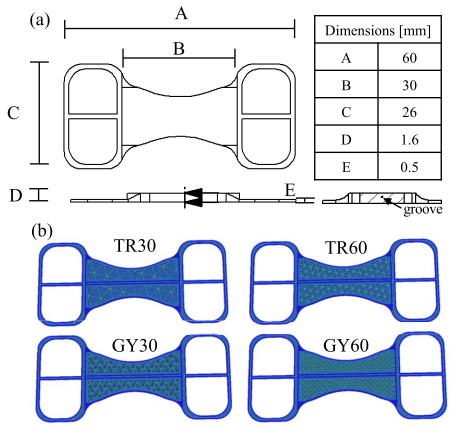

Fig. 1. (a) Size of the 3-D-printed sensors. (b) CURA projects.

reason, after a detailed description of the design and manufacturing processes of the four 3-D-printed sensors proposed in Section III, a further description of the sensors' metrological properties in terms of their response to ε, T, and RH is provided in Section IV.

III. Design and Manufacturing of the 3-D-Printed Sensors Based on FBG Technology

A total of four 3-D-printed sensors were manufactured in TPU by the fused deposition modeling (FDM) technique to investigate the influence of 30% and 60% infills with triangular (TR30 and TR60, respectively) and gyroid (GY30 and GY60, respectively) patterns.

A. Printing Material and Settings Used to Develop the 3-D-Printed Sensors

TPU is a flexible material belonging to the family of thermoplastic elastomers. It is highly durable and easier to extrude than other flexible filaments. In this study, we used TPU with a hardness of 95 Shore A (TPU 95A) since it is one of the most used flexible filaments and is easily printable by a wide range of 3-D printers [28].

After selecting the filament, the 3-D printing technique requires to carefully choose printing settings for conferring specific structural properties to the 3-D specimens. In this study, we used two different patterns (TR and GY) and infill percentages (30% and 60%) to clearly appreciate their influence on the sensors' response. We focused on TR since it is one of the most used and stronger infill patterns in which the grid assumes the shape of a triangle. In addition, we investigated GY since it provides all-around stability, strength, and flexibility to the 3-D models in all directions. It is characterized by a sinusoidal trend which allows obtaining an isotropic pattern [29], [30], [31].

The structural differences between TR and GY, schematically represented in Fig. 1(b), are expected to impact the mechanical properties of the prints and allow a better examination of the influence of the pattern on the FBG response when infills remain equal. In the same way, infills of 30% and 60% were chosen to evaluate the influence of solid percentage on the performance of the sensors when the pattern remains the same. These values are in the range of percentages often recommended for prints.

B. Design of the 3-D-Printed Sensors

The design of the sensors was guided by the necessity to both have the same geometries (to analyze the influence of printing settings on the sensors' performance) and an acceptable wearability (to test the sensors in a scenario of physiological monitoring). The chosen shape has a tighter central constriction with two clampable ends (see Fig. 1).

The overall dimensions of the 3-D structure are 60 mm in length and 26 mm in width, with a height of 1.6 mm for the central part and 0.5 mm for the two ends.

A grooved channel with dimensions of 30 mm $\times$ 0.25 mm $\times$ 0.2 mm was also designed to encapsulate the FBG sensor within the print. The FBG embedding height in the whole printed structure is 1 mm from the lower face and 0.6 mm from the upper face of the 3-D print. Solidworks 2021 was used to design the sensor and CURA software to customize print settings in terms of pattern and infill density. The shape and dimensions of the 3-D-printed sensors and the four configurations used to investigate the influence of the infill properties on the FBG response (TR30, TR60, GY30, GY60) are shown in Fig. 1(a) and (b).

C. Manufacturing Procedure of the 3-D-Printed Sensors

Each sensor was developed by the following five main steps (see Fig. 2).

1) The designed model is imported into the 3-D printer program.
2) The printing is performed. For this study, we used Ultimaker 2+ with TPU 95A filament.
3) When half of the groove structure is completed, the printing program is suspended, and the FBG is positioned in the structure. Two couples of round magnets were used to clap the fiber ends and maintain the FBG in a straining state.
4) Subsequently, printing is resumed, and the FBG is embedded into the structure. The encapsulation of the FBG within the structure is facilitated by the manufacturing technique (i.e., FDM).
5) At the end of the printing procedure, the 3-D-printed sensor is detached from the printer plate with a spatula.

The same process was repeated four times (one time for the sensor) by changing the printer settings according to the chosen patterns and infill percentages. TR30 and GY30 embed an FBG with a nominal λ_B of 1540 nm, while TR60 and GY60 embed an FBG with a nominal λ_B of 1545 nm. All the gratings are 10 mm in length with a reflectivity $>90\%$.

IV. Metrological Characterization of the 3-D-Printed Sensors Based on FBG Technology

When encapsulated, the FBG response is influenced by the mechanical, thermal, and hygroscopic properties of the

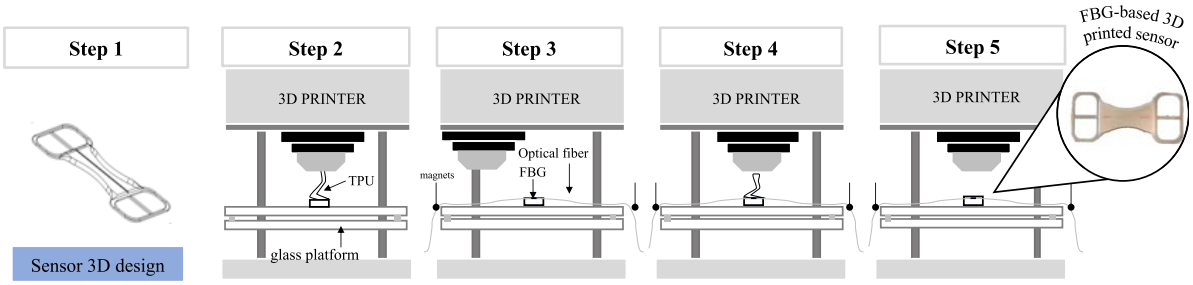

Fig. 2. Fabrication process followed for the manufacturing of the four 3-D-printed sensors from the design model imported into the 3-D-printed program (step 1) to the removal of the printed sensor from the glass platform (step 5).

TABLE I
RESULTS OF THE STATIC CALIBRATION: INFLUENCE OF PATTERNS AND INFILLS ON THE VALUES OF SENSITIVITY TO ε, T, AND RH

	30 %			60 %		
	S_ε [nm/mε]	S_T [nm/°C]	S_{RH} [nm/%RH]	S_ε [nm/mε]	S_T [nm/°C]	S_{RH} [nm/%RH]
GY	$3.2{\cdot}10^{-1}$	$4.8{\cdot}10^{-2}$	$2.1{\cdot}10^{-3}$	$2.9{\cdot}10^{-1}$	$5.4{\cdot}10^{-2}$	$2.4{\cdot}10^{-3}$
TR	$3.9{\cdot}10^{-1}$	$4.9{\cdot}10^{-2}$	$2.3{\cdot}10^{-3}$	$3.6{\cdot}10^{-1}$	$5.4{\cdot}10^{-2}$	$2.6{\cdot}10^{-3}$

hosting material. For this reason, we performed a metrological characterization of the four developed sensors.

This section investigated the sensitivity to ε (S_ε), T (S_T), and RH (S_{RH}). Moreover, we also evaluated the hysteresis errors (h_{err}) since some of the activities of interest (e.g., breathing and heart beating as well as the joint movement repetitions during rehabilitation procedures or training) have a pseudo-periodical pattern.

A. Response of the 3-D-Printed Sensors to Strain

A static assessment of the sensors was carried out to analyze the influence of pattern and infill density on the 3-D sensors' response to ε. Each sensor was positioned between the lower and upper clamps of a tensile machine (Instron 3365).

Quasi-static conditions were guaranteed by a low displacement rate (i.e., 1 mm/min). A $\varepsilon_{\max}$ of about 1% of the sample starting distance between the clamps (i.e., 17 mm) was applied. The displacement induced by the tensile machine on the 3-D sensor during the trial was recorded at the sampling frequency of 100 Hz. The same value of frequency was used to record $\Delta\lambda_B$ values by using an optical spectrum interrogator (si255 based on HYPERION platform; LUNA Inc.). This mechanical test was performed ten times to investigate the repeatability of the system response to the applied ε. Raw data were processed in a MATLAB environment through a custom algorithm to synchronize the recorded signals and extract the calibration curve ($\Delta\lambda_B$ versus ε) for all the sensors. For each FBG, the mean value of $\Delta\lambda_B$ over the ten tests was calculated. At the same time, the expanded uncertainty was obtained as the standard uncertainty multiplied by the coverage factor, considering a t-Student distribution with nine degrees of freedom and a confidence level of 95%. The calibration curve was estimated as the best fitting line (see Fig. 3 and listed values in Table I).

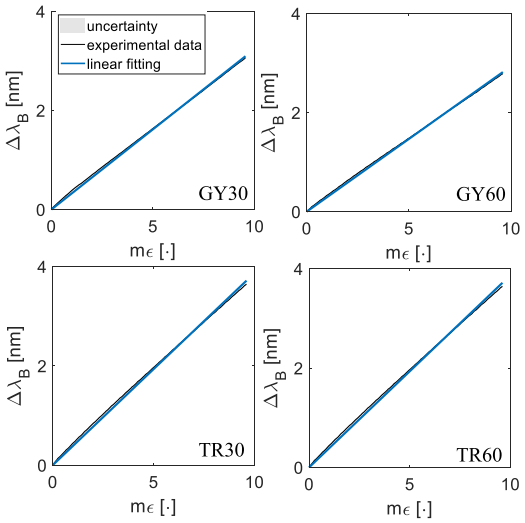

Fig. 3. Calibration curve $\Delta\lambda_B$ versus ε of GY30, GY60, TR30, and TR60. Experimental data (black line), linear fitting (blue line), and uncertainty (shadow area) are shown.

Results showed a linear trend for all four sensors. Therefore, S_ε is considered equal to the slope of the best fitting line. Sensors with a T pattern showed higher S_ε values.

At the same time, infills of 60% led to S_ε values ~4 times lower than the value of a not-encapsulated FBG sensor (i.e., 1.1 nm/mε as provided by the manufacturer).

B. Response of the 3-D-Printed Sensors to Temperature

For the analysis of sensors' response to T, all the sensors were placed within a laboratory oven (PN120 Carbolite Gero[2] and exposed to a ΔT of ~18 °C (i.e., T ranging from ~20 °C to ~38 °C). The test was carried out as follows:

[2]Registered trademark.

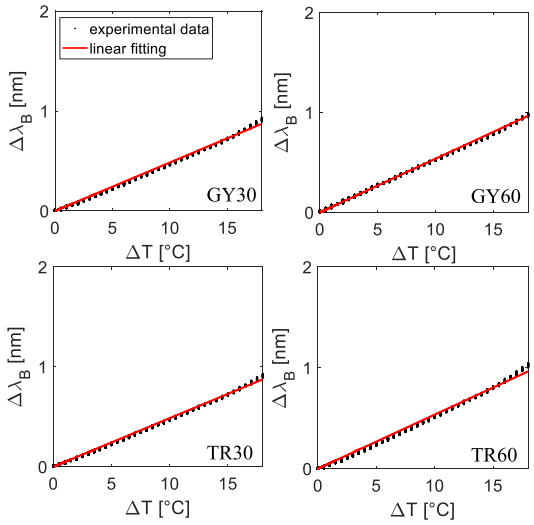

Fig. 4. Calibration curve $\Delta\lambda_B$ versus ΔT of GY30, GY60, TR30, and TR60. Experimental data (black dots) with the linear fitting (red line) are shown.

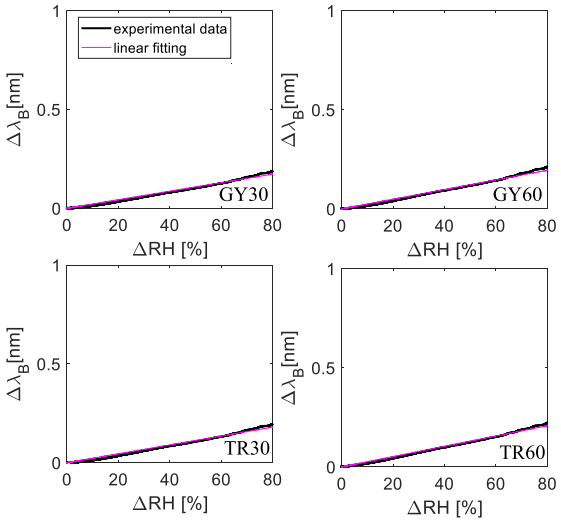

Fig. 5. Calibration curve $\Delta\lambda_B$ versus ΔRH of GY30, GY60, TR30, and TR60. Experimental data (black line) with the linear fitting (magenta line) are shown.

once the maximum value of T was reached, the oven was switched off, and data were collected until T reached the ambient temperature (for approximately ∼7 h) to guarantee a static assessment. Reference values of T were recorded by a thermistor (EL-USB-TP-LCD, EasyLog, Lascar Technology) at a sampling frequency of 5 Hz, and the output of the sensors by the FBG interrogator (FS22, HBM FiberSensing, S.A., Moreira, Portugal) at 1 Hz. Data were analyzed to retrieve the calibration curve $\Delta\lambda_B$ versus ΔT as the best fitting curve. Results showed a linear response for all four sensors. The S_T values are considered equal to the slope of the linear fitting (trends are shown in Fig. 4 and values are listed in Table I).

There was no notable difference in the T response with the pattern, while higher S_T values were reached for 60% of infills. All the S_T values are ∼5 times higher than the one of a not-encapsulated FBG sensor (i.e., 0.01 nm/°C as provided by the manufacturer).

C. Response of the 3-D-Printed Sensors to RH

To investigate the sensors' response to RH, all the sensors were placed inside a custom climatic chamber with a bare polyimide-coated FBG sensor and exposed to slow RH changes. The RH value ranged from ∼15% to ∼95% by forcing the air humidified by the heated humidifier (MR850, Fisher and Paykel Healthcare) from a mass flow controller (EL-Flow, Bronkhorst High-Tech) to the chamber at 1 L/min. A capacitive-based RH sensor (HIH 4000-002, commercialized by Honeywell International Inc., Morristown, NJ, USA) was used to detect the reference RH values. Both $\Delta\lambda_B$ and RH values were collected at 100 Hz. The 3-D sensors' output was recorded by using an FBG interrogator (si255 based on HYPERION platform, LUNA Inc.), and the output of the reference instrument was recorded by using a data acquisition board (NI DAQ USB-6009, NI Instruments) and a LabVIEW interface for the real-time tracking of the RH instantaneous level inside the chamber. Results showed slightly higher values of S_{RH} for infills of 60%. No considerable differences were found with the pattern (see Fig. 5 and listed values in Table I).

All the S_{RH} values are ∼4 times higher than the one experienced by the bare FBG sensor when exposed to the same RH range inside the chamber (i.e., 0.0007 nm/%RH), confirming the hygroscopicity of TPU. However, the S_{RH} values of the 3-D-printed sensors are one and two orders of magnitude lower than S_T and S_ε, respectively; hence, the effect of RH on the sensors' output can be considered negligible (see Table I).

D. Hysteresis of the 3-D-Printed Sensors

The tensile testing machine (Instron mod. 3365) was also used to investigate the h_{err} of the four sensors.

Given several application scenarios, this study pointed out the physiological monitoring with particular regard to the monitoring of cardiorespiratory activity. Considering the dynamics of the respiratory and cardiac activities, eight hysteresis cycles were performed at two speeds mimicking physiological respiratory rate (RR) of 12 breaths per minute (bpm) and heart rate (HR) of 70 beats per minute (bpm), respectively. The outputs of the 3-D-printed sensors and the tensile testing machine were collected at the sampling frequency of 100 Hz.

The eight hysteresis cycles for the four sensors (GY30, GY60, TR30, TR60) are shown in Fig. 6. The h_{err} of each cycle was obtained as follows:

$$h_{\mathrm{err}} = \frac{(\Delta\lambda_B{}^a - \Delta\lambda_B{}^d)^{\max}}{\Delta\lambda_B{}^{\max}} \cdot 100. \tag{3}$$

The superscript "a" indicates the ascending phase, "d" is the descending phase, and "max" is the maximum value of the output recorded during the cycle. Then, the mean value of h_{err} for each sensor and the standard deviation (std) over the eight cycles at RR and HR values were calculated. Results are listed in Table II. Both pattern and infills influenced the hysteresis behavior of the four 3-D-printed sensors. Focusing

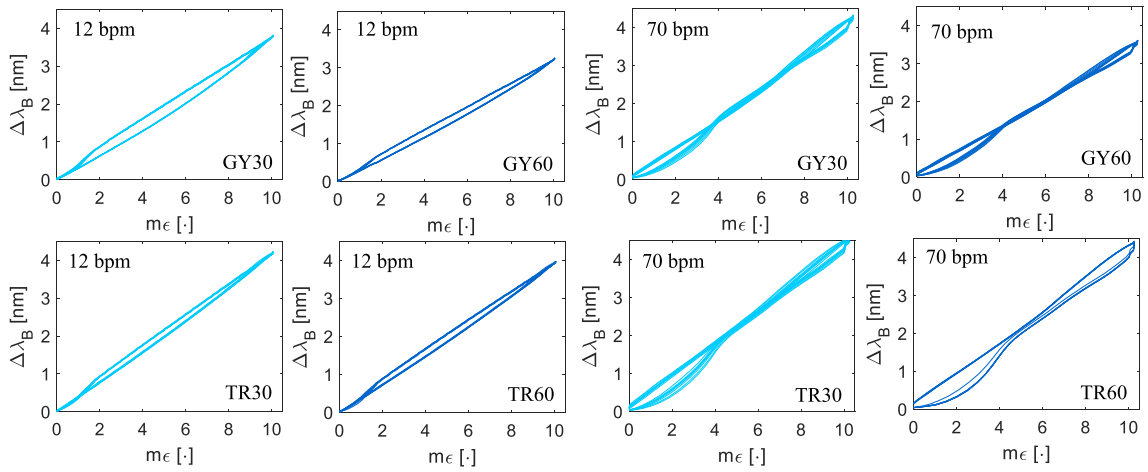

Fig. 6. Hysteresis curves for GY30, GY60, TR30, and T6R0 at velocities mimicking 12 and 70 bpm.

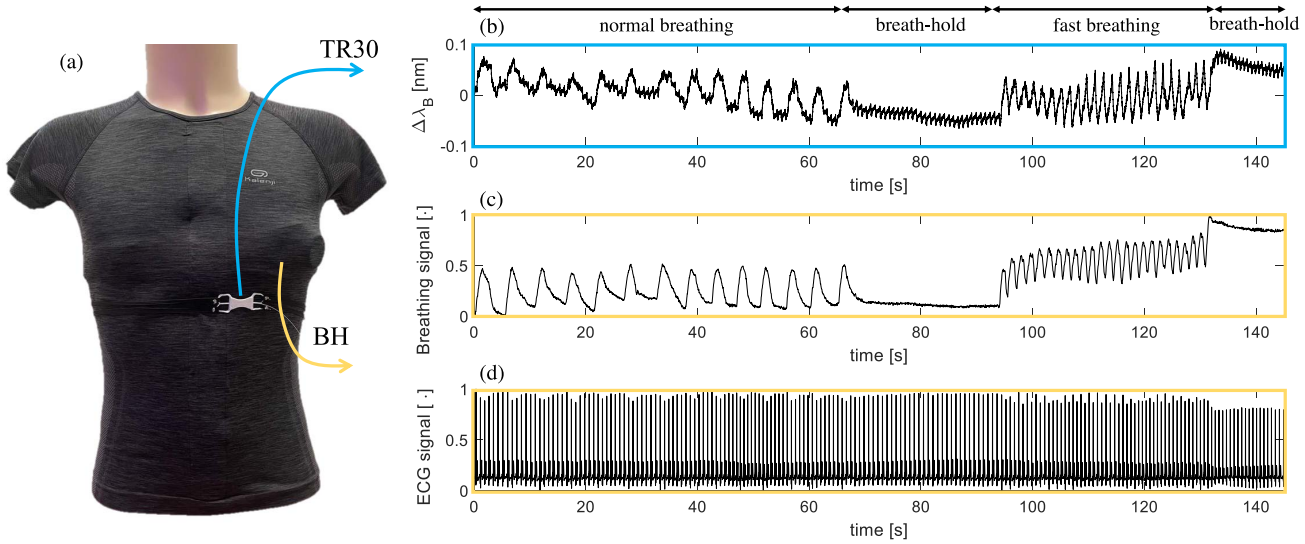

Fig. 7. (a) Sensors placement. (b) Trends of TR30 over time. The trends of the (c) reference breathing and of the (d) ECG sensors recorded by the Bioharness (BH). Normal breathing, breath-hold and fast breathing stages are shown.

TABLE II
HYSTERESIS ERRORS IN PERCENTAGE EXPRESSED AS MEAN ± STD

	30%		60%	
	12 bpm	70 bpm	12 bpm	70 bpm
GY	8.7 ± 0.2%	13 ± 1%	4.3 ± 0.3%	11 ± 1%
TR	5.6 ± 0.3%	11.9 ± 0.7%	4.8 ± 0.3%	10.4 ± 0.2%

on the pattern, generally, GY experienced higher h_{err} (see Table II). Focusing on the influence of infills when the pattern is the same: 60% of infills showed lower h_{err} values than 30%.

These results can be explained considering the different mechanical properties conferred to the prints by the chosen pattern and the infill percentage: the higher the flexibility, the bigger the h_{err} value. When infill is fixed, GY confers higher flexibility than TR. When the pattern is fixed, infills of 30% lead to a more flexible structure.

V. PRELIMINARY TESTS DURING BREATHING AND CARDIAC ACTIVITIES

The use of wearables for RR and HR monitoring is considered of pivotal importance to assess the functioning of the cardiorespiratory system. For this investigation, we chose TR30 from the set of the developed 3-D-printed sensors, since it has the highest S_ε and low h_{err} values. Moreover, the infill of 30% confers to the embedded sensor's low S_T and S_{RH} values. These properties make TR30 suitable for monitoring breathing and cardiac activities when in contact with the chest without any considerable influence of T and RH on the FBG output. The anchorage of TR30 was performed by using two elastic bands inserted into the sensor ends. The sensing element was placed on the left sternum [see Fig. 7(a)].

A volunteer (32-year-old male subject) was invited to wear the system and perform the following protocol: to breath normally for ∼60 s, to hold the breath for ∼20 s, and to breath quickly for ∼30 s (preclinical trial titled Smart Textile—Università Campus Bio-Medico di Roma, protocol number ST-UCBM 27.2(18).20 OSS granted by the Ethical Committee of Università Campus Bio-Medico di Roma, Rome, Italy).

Data from TR30 were recorded using the FBG interrogator at a sampling rate of 1000 Hz, while the reference breathing and ECG waveforms using the Zephyr[1] Bioharness-BH 3 (commercialized by Medtronic) at 25 and 250 Hz, respectively. Fig. 7(b) shows the raw signal recorded by TR30, while Fig. 7(c) and (d) shows the raw signals recorded by the reference breathing and ECG sensors embedded into the BH. Results of the pilot test showed the capability of TR30 to record cardiorespiratory activity. The TR30 trend over time [see Fig. 7(b)] showed the contribution of both breathing and heart beating on the FBG output changes. As expected, chest wall motions during breathing comprise deformations caused by both respiratory and cardiac activities. The cardiac contributions to the TR30 signal are clearly identifiable during the breath-hold stages in the form of a pseudo-periodic $\Delta\lambda_B$ with a small amplitude and fast dynamics. During this phase, the breathing contributions are automatically discharged since the volunteer holds the breath, and the cardiac activity is the main responsible for the TR30 output changes. In contrast, the cardiac contribution during breathing appears as a high-frequency signal over the bigger and slower sinusoidal waves characterizing the breathing activity. These preliminary findings confirmed the high potentiality of TR30 to simultaneously measure breathing and cardiac signals, making this sensor very suitable for future investigations in the field.

VI. Discussion

This work aimed at developing 3-D-printed sensors based on FBG technology for assessing the influence of two main infill properties (i.e., pattern and density) on the sensor metrological properties. In particular, two patterns (TR and GY) and infills (30% and 60%) were chosen to obtain four different printing profiles. As expected, the structural properties of each 3-D-printed sensor influence the response of the FBG inside. Focusing on the pattern, higher S_ε values were found for TR while the values of S_T and S_{RH} suggest no considerable influence of the pattern on the FBG response to T and RH. However, it may be possible to add an FBG outside the structure to avoid output changes due to ε and compensate for the effects of these two other parameters. Since both cardiac and respiratory phenomena are periodic, we investigated the h_{err} values affecting the proposed sensors. This analysis confirmed the higher performance of the TR pattern than GY (see Tables I and II). Regarding the influence of infill density, a value of 30% confers higher S_ε and lower S_T values while no considerable differences were found in the FBG response to RH. Slightly higher values of h_{err} were experienced by sensors with infills of 30% than 60%. Finally, we selected the sensor with the highest S_ε (i.e., TR30) to develop a wearable system based on FBG technology for cardiorespiratory monitoring. The preliminary results confirmed the high potentiality of the proposed technological solution to monitor the chest wall deformations induced by breathing and heart beating simultaneously.

In the literature, most of the works used more rigid printing filaments than TPU like polylactic acid (PLA) or acrylonitrile butadiene styrene (ABS) [32], [33], [34]. For instance, in [32], a 3-D-printed wearable hoop was manufactured in PLA and used for strain sensing. Results showed an S_ε of 4×10^{-2} nm/mε. This value is one order of magnitude lower than the one in the present study, suggesting higher strain sensing performance for the 3-D-printed sensors described in this work. Only a few studies investigated the influence of infill density on the ε, T, and force response of an FBG embedded within a 3-D-printed structure. In [23], three sensors were manufactured in ABS with infills of 20%, 65%, and 99% to investigate the influence of infill density on the FBG response to T and force. Despite the difference in the thermal properties between ABS and the material used in the present study (TPU), results showed that the 3-D-printed sensors have S_T values higher than the one of a not-encapsulated FBG and that these values increase with density. An opposite trend was found in terms of force response: the higher the infill density, the lower the force sensitivity. The importance of assessing the influence of infill density on the response of a wearable system for cardiorespiratory monitoring was investigated in [24]. A flexible material was chosen as printing filament, and infills of 20%, 60%, and 100% were set as density values. Results are in line with our study: the lower the infill density, the higher the S_ε (i.e., S_ε of 1.9×10^{-1} nm/mε in [24] and of 3.9×10^{-1} nm/mε in the present study for the 3-D-printed sensor with the lowest infill density). By comparing strain sensing performance between the sensors in [24] than the one in the present study, FBG in TPU material reached higher strain sensitivity. In addition, we also investigated the influence of two influencing quantities (T and RH) on the FBG response. This analysis was carried out to better evaluate the sensor performance in a real-world scenario. Indeed, both body temperature and sweating may be experienced by the user wearing the proposed sensor, and environmental T and RH changes may also occur. Finally, we investigated the influence of another important printing setting (i.e., the infill pattern) on the performance of the sensors, while the study in [24] did not consider these aspects. Conversely to the manufacturing process in [23] and [24], we proposed a novel fabrication method to improve the repeatability in the fabrication process, making the fiber encapsulation more controllable. Moreover, given the higher performance of the proposed sensors in ε sensing compared to the ones in [24], it is reasonable to assert that this fabrication process may allow a higher bond strength between the optical fiber and the printed structure.

VII. Conclusion

This study showed that the printing profile and the way in which the optical fiber is embedded within the printed structure have a considerable influence on the sensor response. Future studies will be devoted to deeply investigate the influence of these factors on the sensors' response by choosing a higher

number of infill densities and patterns. Moreover, 3-D finite element numerical analysis will be conducted to study the influence of different packaging configurations on the sensor response and finely tune the 3-D print design accordingly. As a result, a knowledge improvement about the relationship between 3-D printing techniques and sensor performance will be achieved, opening up the possibility of teasing out even more appropriate sensor configurations.

ACKNOWLEDGMENT

D. Lo Presti, C. Massaroni, and E. Schena are with the Unit of Measurements and Biomedical Instrumentation, Università Campus Bio-Medico di Roma, 00128 Rome, Italy (e-mail: d.lopresti@unicampus.it; c.massaroni@unicampus.it; e.schena@unicampus.it).

C. Leitão, C. Tavares, and P. Antunes are with i3N, Physics Department, University of Aveiro, 3810-193 Aveiro, Portugal (e-mail: catia.leitao@ua.pt; catia.tavares@ua.pt; pantunes@ua.pt).

A. Noccaro and D. Formica are with the Neurorobotics Group, Newcastle University, Newcastle Upon Tyne NE1 7RU, U.K. (e-mail: alessia.noccaro@newcastle.ac.uk; domenico.formica@newcastle.ac.uk).

M. A. Caponero is with the Photonics Micro and Nanostructures Laboratory, ENEA, 00044 Frascati, Italy (e-mail: michele.caponero@enea.it).

The tensile testing machine (Instron mod. 3365) was also used to investigate the h_{err} of the four sensors.

REFERENCES

[1] T. Erdogan, "Fiber grating spectra," *J. Lightw. Technol.*, vol. 15, no. 8, pp. 1277–1294, Aug. 1997, doi: 10.1109/50.618322.

[2] M. Majumder, T. K. Gangopadhyay, A. K. Chakraborty, K. Dasgupta, and D. K. Bhattacharya, "Fibre Bragg gratings in structural health monitoring-present status and applications," *Sens. Actuators A, Phys.*, vol. 147, no. 1, pp. 150–164, 2008, doi: 10.1016/j.sna.2008.04.008.

[3] D. L. Presti *et al.*, "Fiber Bragg gratings for medical applications and future challenges: A review," *IEEE Access*, vol. 8, pp. 156863–156888, 2020, doi: 10.1109/ACCESS.2020.3019138.

[4] D. Lo Presti *et al.*, "Cardio-respiratory monitoring in archery using a smart textile based on flexible fiber Bragg grating sensors," *Sensors*, vol. 19, no. 16, p. 3581, 2019, doi: 10.3390/s19163581.

[5] N. Agrawal *et al.*, "Detection of L-cysteine using silver nanoparticles and graphene oxide immobilized tapered SMS optical fiber structure," *IEEE Sensors J.*, vol. 20, no. 19, pp. 11372–11379, Oct. 2020, doi: 10.1109/JSEN.2020.2997690.

[6] Z. Wang, R. Singh, C. Marques, R. Jha, B. Zhang, and S. Kumar, "Taper-in-taper fiber structure-based LSPR sensor for alanine aminotransferase detection," *Opt. Exp.*, vol. 29, no. 26, p. 43793, Dec. 2021, doi: 10.1364/oe.447202.

[7] K. S. C. Kuang, R. Kenny, M. P. Whelan, W. J. Cantwell, and P. R. Chalker, "Embedded fibre Bragg grating sensors in advanced composite materials," *Compos. Sci. Technol.*, vol. 61, no. 10, pp. 1379–1387, Aug. 2001, doi: 10.1016/S0266-3538(01)00037-9.

[8] D. Kinet, P. Mégret, K. W. Goossen, L. Qiu, D. Heider, and C. Caucheteur, "Fiber Bragg grating sensors toward structural health monitoring in composite materials: Challenges and solutions," *Sensors*, vol. 14, no. 4, pp. 7394–7419, 2014, doi: 10.3390/s140407394.

[9] H. Montazerian, A. Rashidi, A. S. Milani, and M. Hoorfar, "Integrated sensors in advanced composites: A critical review," *Crit. Rev. Solid State Mater. Sci.*, vol. 45, no. 3, pp. 187–238, May 2020, doi: 10.1080/10408436.2019.1588705.

[10] H. Rocha, C. Semprimoschnig, and J. P. Nunes, "Sensors for process and structural health monitoring of aerospace composites: A review," *Eng. Struct.*, vol. 237, Jun. 2021, Art. no. 112231, doi: 10.1016/j.engstruct.2021.112231.

[11] C. H. Tan, Y. G. Shee, B. K. Yap, and F. R. M. Adikan, "Fiber Bragg grating based sensing system: Early corrosion detection for structural health monitoring," *Sens. Actuators A, Phys.*, vol. 246, pp. 123–128, Aug. 2016, doi: 10.1016/j.sna.2017.10.048.

[12] M. Fajkus, J. Nedoma, P. Siska, and V. Vasinek, "FBG sensor of breathing encapsulated into polydimethylsiloxane," *Proc. SPIE*, vol. 9994, Oct. 2016, Art. no. 99940N, doi: 10.1117/12.2241663.

[13] D. L. Presti *et al.*, "Wearable system based on flexible FBG for respiratory and cardiac monitoring," *IEEE Sensors J.*, vol. 19, no. 17, pp. 7391–7398, Sep. 2019, doi: 10.1109/JSEN.2019.2916320.

[14] D. Lo Presti, D. Bianchi, C. Massaroni, A. Gizzi, and E. Schena, "A soft and skin-interfaced smart patch based on fiber optics for cardiorespiratory monitoring," *Biosensors*, vol. 12, no. 6, p. 363, May 2022, doi: 10.3390/bios12060363.

[15] M. Zaltieri *et al.*, "Feasibility assessment of an FBG-based wearable system for monitoring back dorsal flexion-extension in video terminal workers," in *Proc. IEEE Int. Instrum. Meas. Technol. Conf. (I2MTC)*, May 2020, pp. 1–5, doi: 10.1109/I2MTC43012.2020.9128974.

[16] S. He, S. Feng, A. Nag, N. Afsarimanesh, T. Han, and S. C. Mukhopadhyay, "Recent progress in 3D printed mold-based sensors," *Sensors*, vol. 20, no. 3, p. 703, Jan. 2020, doi: 10.3390/s20030703.

[17] W. Yan, S. Ma, H. Wang, and X. Zhang, "Fiber Bragg grating online packaging technology based on 3D printing," *Opt. Laser Technol.*, vol. 131, Nov. 2020, Art. no. 106443, doi: 10.1016/j.optlastec.2020.106443.

[18] M. R. Khosravani and T. Reinicke, "3D-printed sensors: Current progress and future challenges," *Sens. Actuators A, Phys.*, vol. 305, Apr. 2020, Art. no. 111916, doi: 10.1016/j.sna.2020.111916.

[19] M. Fernandez-Vicente, W. Calle, S. Ferrandiz, and A. Conejero, "Effect of infill parameters on tensile mechanical behavior in desktop 3D printing," *3D Printing Additive Manuf.*, vol. 3, no. 3, pp. 183–192, Sep. 2016, doi: 10.1089/3dp.2015.0036.

[20] J. H. Porter, T. M. Cain, S. L. Fox, and P. S. Harvey, "Influence of infill properties on flexural rigidity of 3D-printed structural members," *Virtual Phys. Prototyping*, vol. 14, no. 2, pp. 148–159, Apr. 2019, doi: 10.1080/17452759.2018.1537064.

[21] W. Gao, H. Ota, D. Kiriya, K. Takei, and A. Javey, "Flexible electronics toward wearable sensing," *Accounts Chem. Res.*, vol. 52, no. 3, pp. 523–533, Mar. 2019, doi: 10.1021/acs.accounts.8b00500.

[22] J. Dunn, R. Runge, and M. Snyder, "Wearables and the medical revolution," *Personalized Med.*, vol. 15, no. 5, pp. 429–448, Sep. 2018, doi: 10.2217/pme-2018-0044.

[23] A. G. Leal-Junior, C. Marques, M. R. N. Ribeiro, M. J. Pontes, and A. Frizera, "FBG-embedded 3-D printed ABS sensing pads: The impact of infill density on sensitivity and dynamic range in force sensors," *IEEE Sensors J.*, vol. 18, no. 20, pp. 8381–8388, Oct. 2018, doi: 10.1109/JSEN.2018.2866689.

[24] C. Tavares *et al.*, "Respiratory and heart rate monitoring using an FBG 3D-printed wearable system," *Biomed. Opt. Exp.*, vol. 13, no. 4, p. 2299, Apr. 2022, doi: 10.1364/boe.452115.

[25] M. G. Zubel, K. Sugden, D. J. Webb, D. Sáez-Rodríguez, K. Nielsen, and O. Bang, "Embedding silica and polymer fibre Bragg gratings (FBG) in plastic 3D-printed sensing patches," in *Proc. SPIE*, vol. 9886, Apr. 2016, Art. no. 98860N, doi: 10.1117/12.2228753.

[26] L. Wang, N. Fang, and Z. Huang, "Polyimide-coated fiber Bragg grating sensors for humidity measurements," in *High Performance Polymers-Polyimides Based-From Chemistry to Applications*. Rijeka, Croatia: InTech, 2012, doi: 10.5772/53551.

[27] J. Xiao and Y. Gao, "The manufacture of 3D printing of medical grade TPU," *Prog. Additive Manuf.*, vol. 2, no. 3, pp. 117–123, Sep. 2017, doi: 10.1007/s40964-017-0023-1.

[28] T. Xu, W. Shen, X. Lin, and Y. M. Xie, "Mechanical properties of additively manufactured thermoplastic polyurethane (TPU) material affected by various processing parameters," *Polymers*, vol. 12, no. 12, pp. 1–16, Dec. 2020, doi: 10.3390/polym12123010.

[29] C. Lubombo and M. A. Huneault, "Effect of infill patterns on the mechanical performance of lightweight 3D-printed cellular PLA parts," *Mater. Today Commun.*, vol. 17, pp. 214–228, Dec. 2018, doi: 10.1016/j.mtcomm.2018.09.017.

[30] *(1) The Best Cura Infill Patterns—YouTube*. Accessed: Jul. 14, 2022. [Online]. Available: https://all3dp.com/2/cura-infill-patterns-all-you-need-to-know/

[31] P. Bean, R. A. Lopez-Anido, and S. Vel, "Numerical modeling and experimental investigation of effective elastic properties of the 3D printed gyroid infill," *Appl. Sci.*, vol. 12, no. 4, p. 2180, Feb. 2022, doi: 10.3390/app12042180.

[32] C. Hong, Y. Zhang, D. Su, and Z. Yin, "Development of a FBG based hoop-strain sensor using 3D printing method," *IEEE Access*, vol. 7, pp. 107154–107160, 2019, doi: 10.1109/ACCESS.2019.2933568.

[33] H. Cheng-Yu, Z. Ahmed Abro, Z. Yi-Fan, and R. Ahmed Lakho, "An FBG-based smart wearable ring fabricated using FDM for monitoring body joint motion," *J. Ind. Textiles*, vol. 50, no. 10, pp. 1660–1673, Jun. 2021, doi: 10.1177/1528083719870204.

[34] P. D. Palma, A. Iadicicco, and S. Campopiano, "Study of fiber Bragg gratings embedded in 3D-printed patches for deformation monitoring," *IEEE Sensors J.*, vol. 20, no. 22, pp. 13379–13386, Nov. 2020, doi: 10.1109/JSEN.2020.3004280.

D. Lo Presti (Associate Member, IEEE) received the Ph.D. degree in 2021.

She is currently a Postdoctoral Research Fellow with the Unit of Measurements and Biomedical Instrumentation, Università Campus Bio-Medico di Roma, Rome, Italy. Her main research interests include the design, fabrication, and feasibility assessment of smart systems and wearables based on fiber optics for biomedical applications.

C. Leitão received the Ph.D. degree in 2017.

She is currently a Researcher with the Nanophotonics and Optoeletronics Group, i3N, Physics Department, University of Aveiro, Aveiro, Portugal, and a collaborator of IT Institute. Her research interests include photonic and optoelectronic solutions for biomedical sensing, namely, physiological and biochemical parameters related to stress and cardiovascular diseases.

A. Noccaro (Member, IEEE) received the Ph.D. degree in 2020.

She is currently a Research Associate with the Neurorobotics Group, Newcastle University, Newcastle Upon Tyne, U.K. Her main research interests include robotics, human–robot interaction, and human motor control.

C. Tavares is currently a DAEPHYS Ph.D. Student with the Physics Department, Aveiro University, Aveiro, Portugal, and the I3N. Her current research interests include the development of optical fiber sensors for e-Health solutions.

C. Massaroni (Senior Member, IEEE) received the Ph.D. degree in 2017.

He is an Assistant Professor of Measurements with the Università Campus Bio-Medico di Roma, Rome, Italy. His research interests include the design, development, and test of wearable devices and unobtrusive measuring systems for medical applications.

Dr. Massaroni has been the Chair of the "Wearable Sensors" TC of the Italy Chapter of the IEEE Sensors Council since 2020.

M. A. Caponero is a Researcher with the Photonics Micro and Nanostructures Laboratory, ENEA Research Center of Frascati, Frascati, Italy. His research interests include the development of measuring systems based on fiber optics for applications ranging from civil engineering and high energy physics to medicine and healthcare.

P. Antunes received the Ph.D. degree in 2011.

He is an Assistant Professor with the Physics Department, Aveiro University, Aveiro, Portugal, and a Researcher with the I3N and IT Institutes. His research interests include the study and simulation of optical fiber sensors based on silica and polymeric fibers, for static and dynamic measurements, data acquisition, optical transmission systems, and sensor networks for several applications.

D. Formica (Senior Member, IEEE) received the Ph.D. degree in 2008.

He is currently a Professor of Bioengineering and leading the Neurorobotics Group, School of Engineering, Newcastle University, Newcastle Upon Tyne, U.K. His main research interests include intersection of robotics/mechatronics, neuroscience, and developmental psychology.

E. Schena (Senior Member, IEEE) received the Ph.D. degree in 2009.

He is a Full Professor of Measurements with the Università Campus Bio-Medico di Roma, Rome, Italy. His research interests include the design and assessment of wearable systems for vital signs monitoring.

Dr. Schena was the Chair of the Italy Chapter of the IEEE Sensors Council in 2018.

Open Access funding provided by 'Università "Campus Bio-Medico" di Roma' within the CRUI-CARE Agreement